

# Single-LED-pumped, room-temperature, solid-state maser

Michael Newns,<sup>1</sup> Shirley Xu,<sup>1</sup> Mingyang Liu,<sup>2</sup> Zike Cheng,<sup>1</sup> Yifan Yu,<sup>1</sup> Ziqiu Huang,<sup>1</sup> Max Attwood,<sup>3</sup> and Mark Oxborrow<sup>1</sup>

<sup>1</sup>*Dept. of Materials, Imperial College London, South Kensington Campus, SW7 6AZ, UK*

<sup>2</sup>*Dept. of Physics, Imperial College London, South Kensington Campus, SW7 6AZ, UK*

<sup>3</sup>*Department of Chemistry, Massachusetts Institute of Technology, Cambridge, MA, 02139, USA*

(\*Electronic mail: michael.newns15@imperial.ac.uk; m.oxborrow@imperial.ac.uk)

Through their ability to achieve ‘cryogenic’ levels of noise performance while operating at room temperature, optically-pumped, solid-state (OPSS) masers show great promise as quantum sensors, oscillators, and amplifiers. We here demonstrate maser oscillation in a microwave cavity containing a crystal of pentacene-doped *para*-terphenyl (ptc:ptp) pumped by a single, chip-scale LED. Here, unlike previous work, the size of the pump source no longer dominates the size of the maser system as a whole. This miniaturization is achieved through invasive optical pumping in the form of a waveguide, the tip of which is embedded into the maser crystal. Combining experimental measurements with ray-tracing analysis, we find that our approach offers at least a factor of 2 enhancement in the cooperativity over end-on optical excitation.

## I. INTRODUCTION:

As quantum devices exploiting stimulated emission, room-temperature masers enable applications that cannot tolerate the severe operating constraints associated with the use of current refrigeration technologies. It is known that masers can amplify weak microwave signals with low noise figures<sup>1</sup>, detect extremely weak a.c. magnetic fields<sup>2</sup>, and generate tones at GHz frequencies exhibiting low phase noise<sup>3,4</sup>. It is also understood<sup>5,6</sup> that, for these capabilities to persist at room-temperature, the maser must operate at high co-operativity, such that the rate of stimulated emission greatly exceeds the rate of incoherent transitions associated with thermal noise. From a practical standpoint, room-temperature masers are still more cumbersome than semiconductor-based alternatives due to the size and weight of the electromagnets and/or optical pump light sources required for their operation. This remaining bulk clearly obviates many of the advantages derived from simply overcoming the need for refrigeration.

In the above context, the original series of room-temperature solid-state masers<sup>7–10</sup>, based on optically-pumped pentacene-doped *para*-terphenyl (ptc:ptp), remain attractive. Unlike masers based on other emitters such as NV centres in diamond, no strong applied DC magnetic field is needed. Furthermore, ptc:ptp masers can sustain high cooperativity in bursts lasting several milli-seconds, which is long enough to be useful in technologically important pulsed applications such as radar and spin-echo EPR. Such a zero-field maser is composed of just two essential parts: the maser cavity itself, and its associated optical pump source.

Hitherto, the size, weight and power (‘SWAP’) requirements of a ptc:ptp maser have been dominated by the optical pump source, with the cavity typically being at least an order of magnitude smaller in volume. As ptc:ptp masers are limited thermally to pulsed operation, the optical pump source must provide pulses of high instantaneous power lasting ns to ms. Suitable pulsed light sources require power electronics capable of outputting many amps of current in short pulses into high-impedance output stages, which is typically achieved

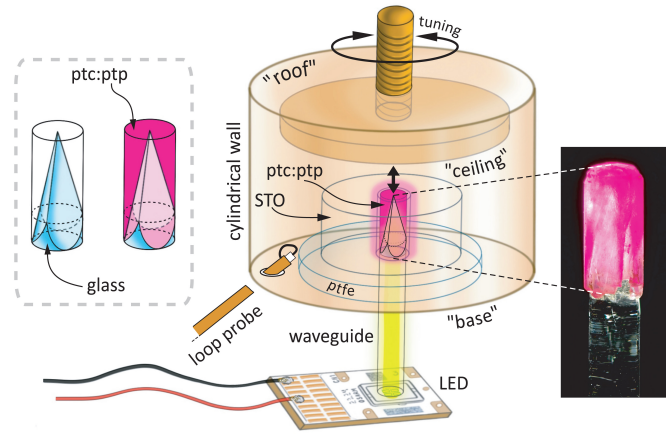


FIG. 1. Geometry of invasively pumped LED maser, including the LED chip, microwave cavity, waveguide and ptc:ptp crystal. The gray-dashed inset box on the then left details the geometry of the waveguide’s 3-faceted tip. Displayed on the right is a photo of the invasively pumped ptc:ptp sample used in this work.

through the discharge of high-voltage capacitors. Such systems are bulky and expensive; the pump sources described in the literature (including pulsed solid-state and dye lasers, Nd:YAG pumped optical parametric oscillators and Xe flash lamps), have typically occupied volumes on the order of 1 m<sup>3</sup> or more (see Fig. 2). The size (and weight) of these pump sources clearly limits the practical application of the masers they drive. To be competitive, ptc:ptp masers must offer either improved performance over existing room-temperature technologies or else SWAP metrics significantly lower than cryogenic alternatives.

Recently, Ng *et al.* demonstrated a mains-powered, shoebox-sized ptc:ptp maser<sup>11</sup> incorporating a miniature pulsed Nd-YAG laser. However, this system still suffers three inefficiencies in common with other (Q-switched and frequency-doubled) Nd:YAG-pumped masers: (1) the 532 nm emission from this laser type lies below (in wavelength) the

primary optical-absorption peak at 589 nm for pentacene (in ptp)<sup>12</sup>; (2) Q-switched lasers generating pulses lasting ns provide sufficient instantaneous optical intensity for the rate of optical stimulated emission (from  $S_1$  back down to ground state  $S_0$ ) to exceed the rate of intersystem crossing ("ISC", from  $S_1$  to  $T_2$ ), thus lowering the triplet yield<sup>13</sup> and (3) due to 0.1% ptc:ptp's short optical penetration depth, shining light onto the outside of a mm-sized ptc:ptp crystal via air-pathed optics will fail to illuminate a substantial fraction of its volume<sup>14</sup>.

Pumping methodologies that attempt to remedy these issues, particularly the use of invasive optical pumping through Ce:YAG luminescent concentrators (LCs)<sup>10,15</sup>, have shown significant increases in maser performance compared to air-pathed laser excitation. However, the low overall efficiency of the LCs used in these systems to date (typically around 2.5 %<sup>16</sup>) has resulted in the need for high-power excitation on the input side of the LC through either bulky xenon flash lamps<sup>10</sup> or arrays of thousands of LEDs<sup>15</sup>.

In this letter, we demonstrate maser action in ptc:ptp using invasive optical pumping from a single, chip scale LED that is commercially available. We find that the same LED plus microwave cavity is incapable of attaining maser threshold when the LED's output is simply 'butt-coupled' to the ptc:ptp crystal (of the same pentacene concentration and molecular crystal quality). We use optical ray-tracing simulations combined with finite-element modeling of the cavity mode to show that this is caused by the direct illumination of the region of strongest magnetic field in the cavity. The resulting maser produces high cooperativity, quasi-continuous maser oscillations showing signs of Rabi-oscillations, and is estimated to produce a magnetic quality factor  $Q_m$  of approximately 3000, competitive with previous ptc:ptp masers<sup>8</sup>.

Our results demonstrate a significant miniaturisation in the volume of the optical pump source used to drive ptc:ptp masers. Compared to previously reported devices in the literature, our maser system is the first for which the size and weight of its optical pump source do not dominate those of the overall maser system. Fig. 2 plots the approximate volume of most of these pump sources. A notable exception is the work of reference 15; this reported another LED-pumped ptc:ptp maser but did not provide sufficient information to estimate the volume that its LEDs occupy. We do know they comprised 2120 LEDs each with an output area of  $1 \text{ mm} \times 1 \text{ mm}$ , for a total output area of  $2120 \text{ mm}^2$ . This work in comparison used an output area of just  $8.32 \text{ mm}^2$ . We attribute this reduction in size to (i) avoiding the loss mechanisms (like escape and re-absorption) associated with Ce:YAG luminescent concentrators<sup>16</sup> and (ii) the effective use of invasive optical pumping.

## II. EXPERIMENTAL SET-UP

In this work, a 0.1% ptc:ptp crystal grown atop a fused-quartz waveguide is used as the maser gain media. An additional, non-invasively pumped crystal and waveguide were also fabricated to help quantify the relative benefit of invasive optical pumping. Schematics of these two geometries are

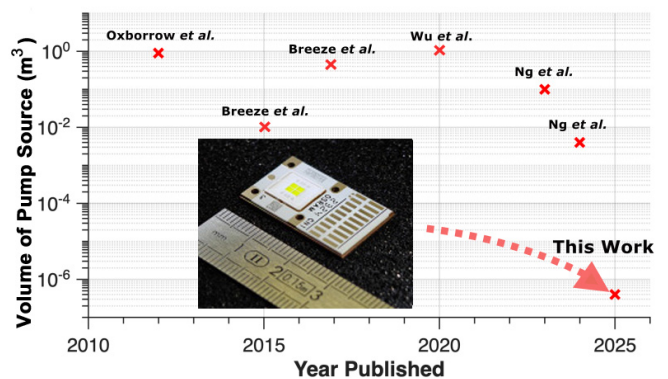


FIG. 2. Approximate optical pump volume reported for key publications on ptc:ptp masers vs year published. The inset photo displays the model of LED used in this work –beside a ruler for scale. References in ascending year are: Oxborrow *et al.*<sup>7</sup>, Breeze *et al.*<sup>8</sup>, Breeze *et al.*<sup>17</sup>, Wu *et al.*<sup>9</sup>, Ng *et al.*<sup>18</sup>, Ng *et al.*<sup>11</sup>.

shown in Fig. 3.

Both waveguides were home-manufactured from 5-mm-diameter fused-quartz rod using traditional lens/prism-making techniques<sup>19</sup>. A cut 13-cm length of rod was held with blocking pitch (85% colophony, 15% beeswax) in a home-made jig (cradle) incorporating angle-defining wedged glass 'waster' plates and pressed against the surface of a rotating grinding/polishing wheel (that received a continuous jet of water for cooling/lubrication) onto which progressively finer grades of abrasive paper were attached. The final polishing of each face/facet was done against a napped cloth impregnated with  $3\text{-}\mu\text{m}$  diamond paste on a similar wheel (that happened to be available; cerium oxide glass-polishing powder would have worked equally well). Both waveguides have simply a polished flat face (oriented at right angles to the rod's axis) at their inputting end –to contact and cover the pump LED's flat outputting face. The 'butt-coupled' waveguide has an identical

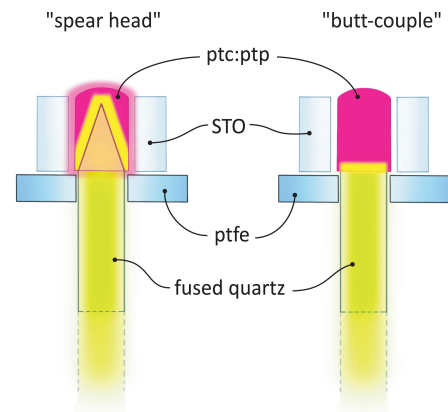


FIG. 3. Meridional cross-sections through the optically-pumped maser's core for the two different pumping geometries considered. In both cases, the STO ring rests on a PTFE washer that itself rests on the cavity's copper base. Yellow shading indicates the extent of pump light penetration.

flat face at its other, outputting end. The outputting end of the ‘spear head’ waveguide in contrast comprises three flat faces (facets), like the apex of a triangular pyramid (tetrahedron), but with a elliptical edge where each of these facets meets the waveguide’s cylindrical shank (see Fig. 1). The waveguide’s length helps isolate the maser crystal from transient magnetic fields generated by the electrical current pulse flowing through the LED; the length could certainly be reduced by placing one or several layers of magnetic (mumetal) shielding between the LED and maser crystal (with a hole for the optical waveguide), but this sophistication was not implemented.

Correspondingly, a ptc:ptp crystal was then grown atop the outputting end of each quartz waveguide by the vertical Bridgman method, as has been described in detail in previous work<sup>9</sup>. Each waveguide was suspended inside its glass growth vial, allowing a ptc:ptp crystal to grow onto and around its outputting end so forming a ‘lollipop’. Note here that the optical waveguide forms part of the mould against/inside which the crystal is grown. A solid [6 mm diameter  $\times$  8 mm height (= axial length)] crystal was grown onto the end of the ‘butt-coupled’ waveguide. A second crystal with the same outer dimensions was grown atop the spear-head waveguide, using the same material and processes.

The maser cavity used in this work, as shown in Fig. 1, closely resembles that used in reference<sup>9</sup>. Made of OFHC copper, it confines the  $TE_{01\delta}$  mode of the  $\text{SrTiO}_3$  (STO) dielectric ring that it surrounds. The prepared ptc:ptp crystal and waveguide enter the cavity from below through a concentric hole in the cavity’s base plate. The mode’s frequency can be adjusted by raising/lowering the height of the cavity’s movable ceiling and is tuned to the 1.4496 GHz frequency of ptc:ptp’s masing  $T_X - T_Z$  transition using a HP 8753A vector network analyser (VNA). An inductive coupling loop ‘probe’, formed from the stripped end of a length of RG402 semi-rigid microwave cable is inserted into the cavity (to which this cable’s outer is electrically grounded). The size and insertion depth of the loop are chosen to render it slightly undercoupled with respect to the  $TE_{01\delta}$  mode from which it extracts modest power for measurement. Upon installing a second extremely undercoupled loop probe (not shown in Fig. 1), the transmission ( $S_{21}$ ) between these two probes is monitored using a VNA, whereby the mode’s frequency and  $Q$  can be ascertained. The  $TE_{01\delta}$  mode’s loaded  $Q$  factor (with waveguide + ptc:ptp crystal inserted into the bore of the STO ring) was measured to be  $Q_L \approx 6000$ . The bottom, flat-faced end of the waveguide is rested onto the output face of the pump LED with a dab of photo-chemically resistant optical coupling fluid (*viz.* ‘Santovac 5’ polyphenyl ether diffusion-pump oil) filling the gap between the two surfaces. The VNA is disconnected from the cavity before the LED is fired. The voltage signal generated by the cavity’s primary (most strongly coupled) loop is directly monitored (at 50- $\Omega$  input impedance) by a Keysight DSOX 6002A 6-GHz oscilloscope (sampling at 5 GSa  $s^{-1}$ ). A double-DC block is inserted between the cavity and scope as a precaution against instrument damage from ‘pilot error’.

The optical source is a single LED chip (OSRAM LE CG P2AQ)<sup>20</sup> producing high-luminance yellow-green 565-

575 nm light, intended for use in video projectors/displays. The LED’s outputting surface is rectangular with dimensions 3.2 mm  $\times$  2.6 mm, which can be fully covered by the flat inputting end of a 5-mm quartz waveguide. The LED is driven by a home-made circuit that discharges a capacitor (EVOX RIFA 22,000  $\mu\text{F}$ , 63 V, low-ESR electrolytic) through a TTL-controlled, low-on-resistance MOSFET switch (*viz.* four IRFB3077PbF transistors in parallel driven by a TC4452VAT gate driver) into the LED in series with a low-inductance 0.02- $\Omega$  resistor for current monitoring. The voltage across this resistor is also used to trigger the monitoring DSOX 6002A oscilloscope. By varying the TTL pulse duration and the voltage to which the capacitor is charged, the resulting pulse energy and duration can be controlled accurately. As a precaution against overheating during sustained pulsed operation the LED is mounted with thermally conductive paste onto the top of a metallic CPU heat sink. The drive currents used in this work are significantly above the maximal surge current (14 A) stated in the LED’s datasheet. The risk of damage was mitigated by using the shortest possible pulse duration (150  $\mu\text{s}$ ) and a low duty cycle (not more than 10 pulses per second). This allowed for hours of above-threshold pulsed operation without LED failure.

The optical output from the LED (both overall energy dose and instantaneous power as a function of time) received by the maser crystal is estimated using a combination of an ES245C pyroelectric energy meter and a DET-200 (modern equivalent: DET100A2) silicon photodetector, both from Thorlabs. The flat receiving surface of the ES245C is placed just above the flat outputting face of a 5-mm fused-quartz waveguide (*i.e.*, the butt-coupled geometry but without a maser crystal) with air in between. The vertical scale of the corresponding time profile recorded by the DET-200 (used as an uncalibrated linear power meter of sufficient bandwidth) is then adjusted such that its integrated area-under-the-curve equals the inferred energy dose; this allows for the instantaneous absorbed power as a function of time to be determined –as are shown at the bottom of Fig. 5 for two different charge voltages on the LED-driver’s capacitor (and thus two different overall pulse energies).

Such a ‘dry’ measurement of the optical energy/power (with an air gap between the outputting face and energy meter) inevitably underestimates the power/energy fraction of the light that will actually get transmitted into the ptc:ptp maser crystal (whose refractive index lies closer to that of fused quartz compared to that of air). To correct for this, ray tracing is used to determine (a) the fraction of the LED’s output that arrives at the surface of the ES245C energy meter and (b) the fraction of same that gets absorbed by the ptc:ptp crystal for both the (i) butt-coupled and (ii) invasive-spear-head geometries. The ray tracing takes into account both reflections from all interfaces and the escape of pump light from the crystal (upon passing through the sections of it that are too thin to completely absorb the pump light). Although the invasive-spear-head geometry does better than a butt couple at avoiding the retro-reflection of pump light back into the waveguide, more pump light is lost by escape through the thin sections of the crystal where the spear head’s flat faces meet the wave-

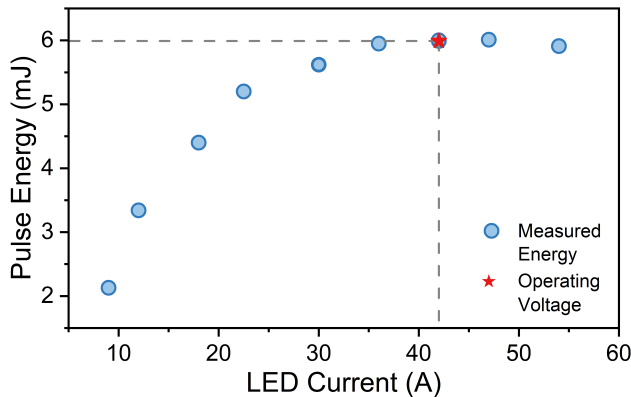


FIG. 4. Detected LED output power vs (maximal) drive current for 150- $\mu$ s pulses.

uide outer cylindrical surface. [The latter problem *could* have been remedied by growing a crystal of slightly greater diameter and/or making the waveguide out of a quartz rod of slightly smaller diameter (like 4.5 mm); neither was implemented.] The ratio of the fractions (b)/(a) provides a correction factor, allowing the true amount (*i.e.*, energy and thus number of photons) of light absorbed by the ptc:ptp crystal to be inferred from the energy meter’s reading. We find the factor to be (i) 1.07 for the butt couple and (ii) 1.01 for the spear head.

### III. OPTICAL AND RF SIMULATIONS

To better understand our results and direct further improvements, we simulate the spatial distribution (density) of absorbed optical energy,  $\rho_{\text{opt}}(\vec{r})$ , within ptc:ptp crystal in units of  $\text{W}/\text{mm}^3$ , for both the invasive and butt-coupled configurations, using PVtrace open source ray tracing software<sup>21–24</sup>. Within our simulation, we treat the LED as a flat rectangular lambertian light source, emitting through a layer of optical coupling liquid into the waveguide. Light from the LED that is successfully captured by the waveguide then propagates along it by total internal reflection until it meets the waveguide’s terminating ptc:ptp crystal. In our simulation, we assume that 0.1% ptc:ptp is a linear optical absorber (obeying the Beer-Lambert law in the direction of optical transport), where the effective absorption coefficient of the light emitted by the LED is  $\approx 2 \text{ mm}^{-1}$  given the LED’s output spectrum<sup>20</sup> and ptc:ptp’s absorption spectrum<sup>18,25</sup>. Neither the birefringence of para-terphenyl nor the anisotropy (both direction and polarization dependence) of pentacene’s optical absorption (when dissolved as a substitutional dopant in the former) were explicitly included. In our invasive-pumping simulations, a simplified two-faced wedge geometry was adopted instead of the experimental three-faced spear-head geometry (though with equivalent aspect ratios). This choice was made to preserve clear and intuitive 2D projections of the absorbed optical energy density, as the non-parallel facets of the three-faced geometry complicate direct visual presentation (with conven-

tional 2D figures). Physically, this simplification is not expected to significantly affect the optical coupling efficiency, since absorption at each emitting facet occurs without total internal reflection and the ray distribution retains azimuthal symmetry.

In tandem with the optical engineering, RF simulations of the a.c. magnetic field generated by the  $TE_{01\delta}$  mode are conducted using eigen-frequency analysis of a (lossless) model of the cavity in COMSOL Multiphysics (version 6.0). The STO resonator is modeled as a lossless dielectric with  $\epsilon_r = 318$ , supported by a ptfe stand, with perfect-electric-conductor boundary conditions simulating the copper cavity’s walls. No attempt is made to electromagnetically simulate the ptc:ptp crystal, waveguide or coupling loop.

### IV. RESULTS

Using the experimental setup described above, maser oscillations of tuneable duration and intensity could be observed on the oscilloscope. When the LED is powered with 42 A (peak) pulses of 150  $\mu$ s duration, it transmits a total energy of 6 mJ per pulse to the pentacene crystal (see Fig. 4). Under these conditions, the strongest maser oscillations were recorded. An example of one such oscillation is presented in Fig. 5. The maser pulse starts approximately 30  $\mu$ s after the LED is provided with current. This is significantly longer than the start-up times of other maser systems reported in the literature<sup>18,26</sup>, which are on the order of a few  $\mu$ s. This increased delay before the start of masing is attributed to turn on delay in the LED as can be seen at the bottom of Fig. 5. The oscillatory output of the maser burst is attributed to Rabi-oscillations, indicative of the pumping scheme being powerful enough to drive the system into the strong coupling regime<sup>17</sup>, where the maser emission is sufficient to overcome both losses and de-phasing.

These Rabi oscillations decay during the signal, although maser emission is visible throughout the 150  $\mu$ s pump duration, and even slightly after. This quasi-continuous wave (quasi-CW) operation has only been reported in two other ptc:ptp maser system<sup>10,15</sup>. This indicates that the LED output maintains sufficient power throughout its duration to drive the maser oscillation, even as the  $T_X : T_Z$  population ratio decreases due to bottlenecking of the  $T_Z$  state<sup>27</sup>.

The transient peak at the end of the maser burst is attributed to electromagnetic interference associated with the LED-driver’s turn off. As can be seen in Fig. 5 (lowest section), there is no detectable effect in the optical output of the LED. The distance between the LED and the maser crystal provided by the waveguide is intended to minimise magnetic interference with the sample, which could be expected from the strong pulsed current in the wires supplying the LED. Noting that the spectrograms show no evidence of this interference within the band of the maser oscillation, the transient is attributed to inductive interference/crosstalk between the high-current LED driver and the maser’s output channel (*i.e.*, the cable connecting the cavity to the oscilloscope’s input stages). More rigorous engineering (including better elec-

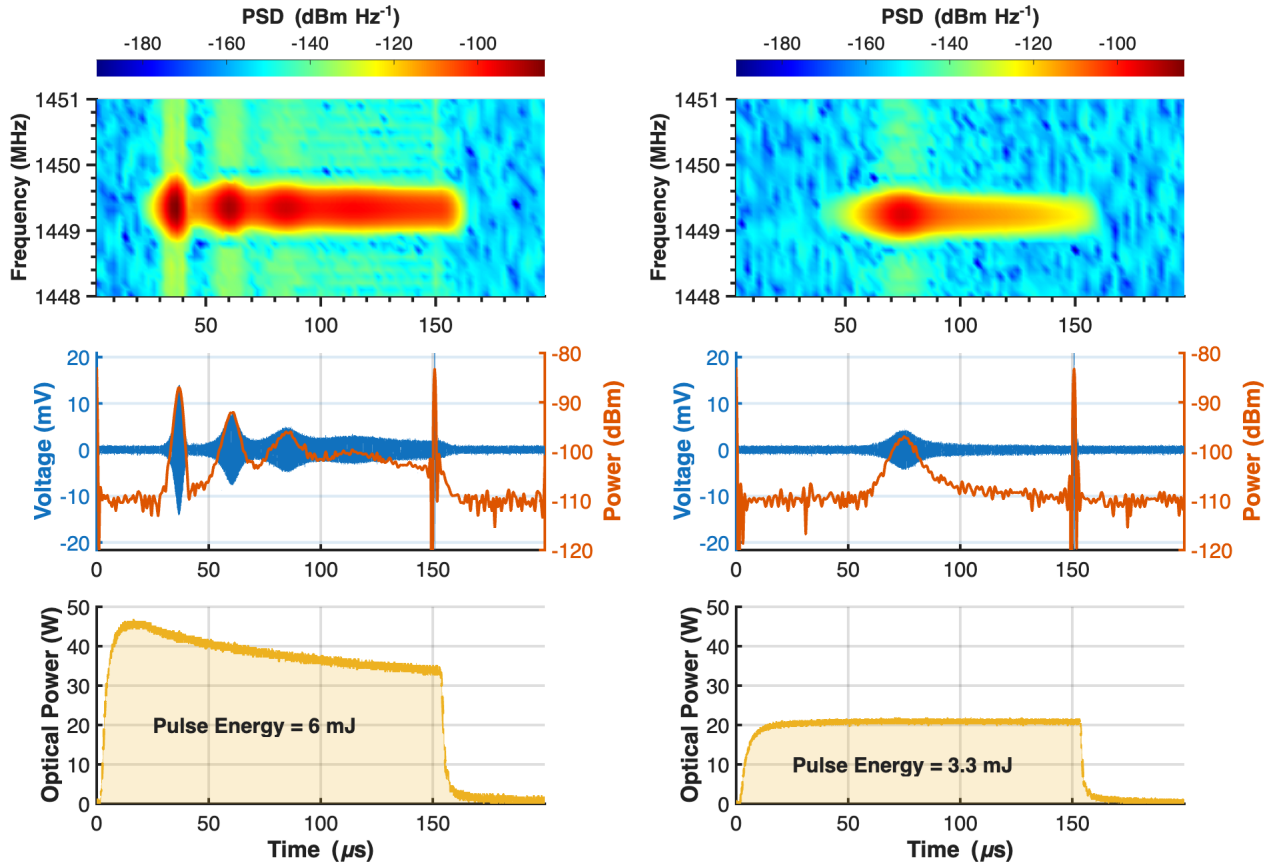


FIG. 5. Maser oscillations produced by the invasively pumped ptc:ptp maser under two different pump intensities. The left column shows the maser bursts recorded at peak LED output power (6 mJ per pulse), whilst the right column shows the maser burst produced when the pump power was reduced to 3.3 mJ per pulse. This was found to be the threshold optical pump power for this sample. The top row shows the power spectral density (PSD, in  $\text{dBm}\cdot\text{Hz}^{-1}$ ), derived from the short-time-Fourier transform of each maser oscillation, using Hamming windows containing  $2.5 \times 10^4$  samples with 50 % overlap, generated in MATLAB R2025B. The middle row shows the voltage trace as detected by the oscilloscope in blue, and the corresponding RMS power envelope in red, taken as an envelope over windows of 3000 samples. The lower rows shows the time profile of the instantaneous optical power supplied by the LED in each case, with the inset indicating the integrated pulse energy.

trical isolation/shielding between systems) would be expected to mitigate the observed spikes.

Reducing the optical output power to an estimated 3 mJ over the same pulse duration results in a much weaker maser burst, which starts after approximately  $60 \mu\text{s}$ , and decays more rapidly. The elongated turn-on time at lower pump power concords with the literature<sup>18,26</sup>, and is also partially explained by the delayed time to maximum optical output at 12 A drive current. The reduction in both the output power of the oscillation and its duration along with the absence of Rabi oscillations is associated with a reduction in cooperativity due to lower pump power. This pump power (corresponding to a drive current of 12 A) was found to be the threshold pump power for masing in this system. Following equation (1), the cooperativity of the system is expected to have a linear dependence on the optical pump power. As such, this result indicates that the previous maser burst (corresponding to a peak

drive current of 42 A) had a cooperativity of approximately 2. For an intrinsic cavity  $Q_0$  of 6,000, this corresponds to a magnetic  $Q_m$  of 3,000. For comparison, reference<sup>8</sup> reports a ptc:ptp maser with a  $Q_m$  of 4,500 in a resonator with a  $Q_L$  of 8,900, producing a comparable cooperativity to this system but by using a (large) shoe-box-sized xenon flash lamp producing a peak optical power of 60-70 W.

When the same system is configured in a ‘butt-coupled’ configuration, with the solid ptc:ptp crystal abutting the flat-ended waveguide (as described above), no maser oscillations were observed, regardless of the optical power provided. This highlights the importance of invasive optical pumping in reaching maser threshold. The maser cooperativity (here denoted as  $\Gamma$ ) is a dimensionless number quantifying the amount by which a maser exceeds threshold ( $\Gamma \geq 1$  for masing). Extending the definition of the maser cooperativity provided in reference<sup>5</sup> to account for spatially uneven optical pumping

gives:

$$\Gamma = \mu_0 \gamma^2 \sigma^2 \times \frac{\Theta_{\text{ISC}}^{\text{eff}} \times T_1^{\text{eff}} T_2^*}{\omega_{\text{opt}}} \times \frac{Q_L \int_{\Sigma} (\rho_{\text{opt}}(\vec{r}) |B(\vec{r})|^2) dV}{\int_{\text{cav}} |B(\vec{r})|^2 dV}; \quad (1)$$

where:  $\mu_0$  is the permeability of free space,  $\gamma$  is the electron gyromagnetic ratio,  $\sigma^2$  is the transition probability matrix element for the maser transition,  $\omega_{\text{opt}}$  is the pump photon angular velocity,  $\Theta_{\text{ISC}}^{\text{eff}}$  is the effective intersystem crossing efficiency,  $T_1^{\text{eff}}$  is the effective spin-lattice relaxation time,  $T_2^*$  is the observed spin-spin relaxation time,  $Q_L$  is the (loaded) resonator's quality factor,  $\rho_{\text{opt}}(\vec{r})$  is the optical energy density at position  $\vec{r}$  in the crystal  $\Sigma$ ,  $B(\vec{r})$  is the resolved component of the magnetic flux density interacting with the sample at position  $\vec{r}$ , and  $B(\vec{r})$  is the complete magnetic flux density at same.

From the point of view of optimising the cooperativity of a given maser system through optical engineering, the integral in the numerator of the final factor of (1) is the main quantity of interest. It is clear that increasing the value of this integral is best achieved by maximizing the optical energy density in those areas of the sample where the RF magnetic field is strong.

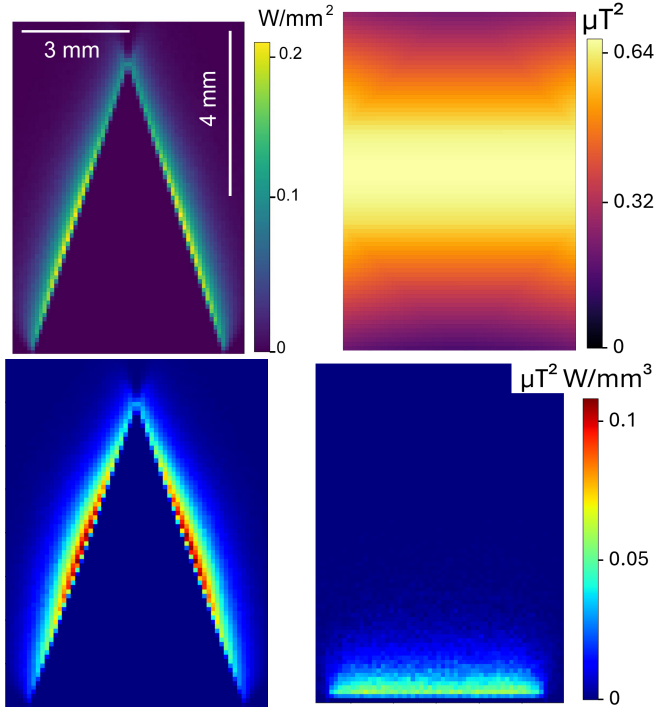


FIG. 6. Top left: Simulation of the normalized absorbed energy density  $\tilde{\rho}_{\text{opt}}$ , in the invasively pumped ptc:ptp sample, using PVtrace. Top right: COMSOL simulation of the normalized  $|\tilde{B}|^2$  inside the bore of the STO dielectric resonator. These are projected from the full 3D data sets. The integral over the displayed region for both  $\tilde{\rho}_{\text{opt}}$  and  $|\tilde{B}|^2$  is normalized to 1 W of total absorbed optical power, and 1 J of total magnetic flux energy, respectively. Bottom panel: Comparison of the local value of  $\tilde{\rho}_{\text{opt}} \times |\tilde{B}|^2$  for invasive pumping (left) and butt-coupling (right).

Examples of the simulated distributions of  $\rho_{\text{opt}}(\vec{r})$ ,  $|B(\vec{r})|^2$  and  $\rho_{\text{opt}}(\vec{r}) \times |B(\vec{r})|^2$  are shown in Fig. 6. Combining optical and RF simulations in this manner allows one to both map the distribution of  $\rho_{\text{opt}}(\vec{r}) \times |B(\vec{r})|^2$  and to estimate the normalised utilization or overlap factor defined as:  $\Delta = \int_{\Sigma} (\tilde{\rho}_{\text{opt}}(\vec{r}) |\tilde{B}(\vec{r})|^2) dV$  which provides a measure of the overall efficiency of the pumping geometry simulated. This term evaluates to  $\Delta = 2.26 \times 10^{-3}$  for the butt-coupled configuration, while for the invasively pumped configuration it evaluates to  $\Delta = 4.60 \times 10^{-3}$ , demonstrating a 2.08 times improvement with invasive pumping. It should be noted that this is despite a large reduction in the available volume of crystal inside the bore of the STO ring for the spear-head geometry. Given that the invasively pumped (spear-head) variant was found to have a cooperativity of approximately 2, this result implies that the butt-coupled variant lies just below the  $\Gamma = 1$  threshold for maser oscillation, consistent with experiment.

We further simulate the limit of completely uniform optical excitation (*i.e.*,  $\rho(\vec{r}) \equiv \bar{\rho}_{\Sigma}$ ), and find this to provide worse performance than that provided by our (imperfect) invasive pumping geometry, with the above integral evaluating to  $\Delta = 4.56 \times 10^{-3}$ . We can thus conclude that, for OPSS masers, in the limit where the total optical power available is insufficient to saturate all optical transitions throughout the crystal, it is preferable to more intensely excite a smaller area of the sample near the region of maximal magnetic flux density. In commercially feasible embodiments of the ptc:ptp maser, we expect this pump-limited regime to hold, and thus conclude that invasive optical pumping would be the preferred excitation geometry.

## V. CONCLUSIONS

We have demonstrated high-cooperativity maser oscillations in a solid-state, room-temperature maser that is invasively pumped through a quartz waveguide by a single, chip-scale LED. We estimate the cooperativity of this maser to be approximately 2, and find it to be capable of quasi-CW maser oscillations. This system is the smallest room-temperature maser yet reported in the literature, and is the first in which the optical pump source is not a limiting component in terms of the maser's overall volume and weight. We find that the same maser system is incapable of achieving masing when butt-coupled to a similar waveguide. Through a novel coupled RF-optical simulation approach, we estimate that the enhancement in cooperativity achieved by the invasive pumping is approximately a factor of 2 compared to end-on pumping, and even a slight improvement over perfectly uniform pumping.

A highly satisfying feature of our work is the agreement between our simulated pumping efficiencies and our experimentally observed pumped thresholds (and co-operativities inferred therefrom) –despite the rather drastic simplifications taken in our optical simulations. In particular we note, on an absolute scale, the ptc:ptp gain medium is still poorly utilized (*i.e.*,  $\Delta \ll 1$ ), suggesting substantial headroom for improvements. Our work motivates the development of more

advanced optical pumping methodologies and more realistic 3D simulations (that include material anisotropy) to further improve the performance of ptc:ptp masers towards providing advantageous devices with widespread applications. Combined with other developments in the maser literature, we expect our work to promote the development of commercially practical devices.

## VI. ACKNOWLEDGMENTS

We thank Ben Gaskill of Gaskill Quartz Ltd., London, for manufacturing the STO ring resonator used in this work.

## VII. BIBLIOGRAPHY

- <sup>1</sup>R. C. Clauss and J. S. Shell, *Ruby masers*, edited by M. S. Reid (JPL Deep Space Communications And Navigation Series, Jet Propulsion Laboratory, 2008).
- <sup>2</sup>H. Wu, S. Yang, M. Oxborrow, M. Jiang, Q. Zhao, D. Budker, B. Zhang, and J. Du, “Enhanced quantum sensing with room-temperature solid-state masers,” *Science Advances* **8**, eade1613 (2022).
- <sup>3</sup>H. M. Goldenberg, D. Kleppner, and N. F. Ramsey, “Atomic hydrogen maser,” *Physical Review Letters* **5**, 361 (1960).
- <sup>4</sup>Y. Varshavsky, O. Zgadzai, and A. Blank, “Solid-state maser with microwatt output power at moderate cryogenic temperatures,” arXiv preprint arXiv:2504.06846 (2025).
- <sup>5</sup>M. Oxborrow and US patent US9608396B2, “Maser assembly,” (2012).
- <sup>6</sup>A. Sherman, O. Zgadzai, B. Koren, I. Peretz, E. Laster, and A. Blank, “Diamond-based microwave quantum amplifier,” *Science Advances* **8**, eade6527 (2022).
- <sup>7</sup>M. Oxborrow, J. D. Breeze, and N. M. Alford, “Room-temperature solid-state maser,” *Nature* **488**, 353–356 (2012).
- <sup>8</sup>J. Breeze, K. J. Tan, B. Richards, J. Sathian, M. Oxborrow, and N. M. N. Alford, “Enhanced magnetic Purcell effect in room-temperature masers,” *Nature Communications* **6**, 1–6 (2015).
- <sup>9</sup>H. Wu, H. Wu, S. Mirkhanov, W. Ng, K.-C. Chen, Y. Xiong, Y. Xiong, and M. Oxborrow, “Invasive optical pumping for room-temperature masers, time-resolved EPR, triplet-DNP, and quantum engines exploiting strong coupling,” *Optics Express* **28**, 29691–29702 (2020).
- <sup>10</sup>H. Wu, X. Xie, W. Ng, S. Mehanna, Y. Li, M. Attwood, and M. Oxborrow, “Room-Temperature Quasi-Continuous-Wave Pentacene Maser Pumped by an Invasive Ce:YAG Luminescent Concentrator,” *Physical Review Applied* **14** (2020).
- <sup>11</sup>W. Ng, Y. Wen, M. Attwood, D. C. Jones, M. Oxborrow, N. M. N. Alford, and D. M. Arroo, “‘Maser-in-a-shoebox’: A portable plug-and-play maser device at room temperature and zero magnetic field,” *Applied Physics Letters* **124**, 44004 (2024).
- <sup>12</sup>Q. Ai, P. Chen, Y. Feng, and Y. Xu, “Growth of Pentacene-Doped p-Terphenyl Crystals by Vertical Bridgman Technique and Doping Effect on Their Characterization,” *Crystal Growth and Design* **17**, 2473–2477 (2017).
- <sup>13</sup>K. Takeda, T. Yamamura, A. Kagawa, and M. Kitagawa, “Enhancement of efficiency in photo-excitation to the triplet state by laser-pulse reshaping,” *Journal of Magnetic Resonance* **174**, 310–313 (2005).
- <sup>14</sup>K. Takeda, K. Takegoshi, and T. Terao, “Zero-field electron spin resonance and theoretical studies of light penetration into single crystal and polycrystalline material doped with molecules photoexcitable to the triplet state via intersystem crossing,” *Journal of Chemical Physics* **117**, 4940–4946 (2002).
- <sup>15</sup>S. Long, L. Lopez, B. Ford, F. Balembois, R. Montis, W. Ng, D. Arroo, N. Alford, H. Torun, and J. Sathian, “LED-pumped room-temperature solid-state maser,” *Communications Engineering* **4** (2025).
- <sup>16</sup>J. Sathian, J. D. Breeze, B. Richards, N. M. Alford, and M. Oxborrow, “Solid-state source of intense yellow light based on a Ce:YAG luminescent concentrator,” *Optics Express* **25**, 13714–13727 (2017).
- <sup>17</sup>J. D. Breeze, E. Salvadori, J. Sathian, N. McN. Alford, and C. W. Kay, “Room-temperature cavity quantum electrodynamics with strongly coupled Dicke states,” *npj Quantum Information* **3** (2017).
- <sup>18</sup>W. Ng, X. Xu, M. Attwood, H. Wu, Z. Meng, X. Chen, and M. Oxborrow, “Move Aside Pentacene: Diazapentacene-Doped para-Terphenyl, a Zero-Field Room-Temperature Maser with Strong Coupling for Cavity Quantum Electrodynamics,” *Advanced Materials* **35**, 2300441 (2023).
- <sup>19</sup>F. Twyman, *Prism and Lens Making, Second Edition: A Textbook for Optical Glassworkers* (Taylor and Francis, 1988).
- <sup>20</sup>OSRAM OSTAR™ Projection Power, LE CG P2AQ, ams-OSRAM AG (2025).
- <sup>21</sup>D. J. Farrell, *Characterising the Performance of Luminescent Solar Concentrators*, Ph.D. thesis, Imperial College London (2008).
- <sup>22</sup>D. J. Farrell, “pvtrace: Optical ray tracing for luminescent materials and spectral converter photovoltaic devices,” <https://github.com/danieljfarrell/pvtrace>.
- <sup>23</sup>S. Verma, D. J. Farrell, and R. C. Evans, “Ray-trace modeling to characterize efficiency of unconventional luminescent solar concentrator geometries,” *ACS Applied Optical Materials* **1**, 1012–1025 (2023).
- <sup>24</sup>Shomik Verma, “Pvtrace-Sv,” <https://github.com/shomikverma/pvtrace-sv>.
- <sup>25</sup>K. A. Nelson, D. Lutz, M. Fayer, and L. Madison, “Laser-induced phonon spectroscopy. optical generation of ultrasonic waves and investigation of electronic excited-state interactions in solids,” *Physical Review B* **24**, 3261 (1981).
- <sup>26</sup>E. Salvadori, J. D. Breeze, K. J. Tan, J. Sathian, B. Richards, M. W. Fung, G. Wolfowicz, M. Oxborrow, N. M. N. Alford, and C. W. Kay, “Nanosecond time-resolved characterization of a pentacene-based room-temperature MASER,” *Scientific Reports* **7**, 1–8 (2017).
- <sup>27</sup>H. Wu, W. Ng, S. Mirkhanov, A. Amirzhan, S. Nitnara, and M. Oxborrow, “Unraveling the Room-Temperature Spin Dynamics of Photoexcited Pentacene in Its Lowest Triplet State at Zero Field,” *Journal of Physical Chemistry C* **123**, 24275–24279 (2019).